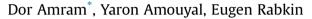
Acta Materialia 102 (2016) 342-351

Contents lists available at ScienceDirect

Acta Materialia

journal homepage: www.elsevier.com/locate/actamat

Encapsulation by segregation – A multifaceted approach to gold segregation in iron particles on sapphire



Department of Materials Science and Engineering, Technion – Israel Institute of Technology, 3200003 Haifa, Israel

ARTICLE INFO

Article history: Received 19 July 2015 Received in revised form 31 August 2015 Accepted 31 August 2015 Available online 8 October 2015

Keywords: Segregation Interfacial segregation Surface energy (anisotropy) Density functional theory (DFT) Particles

ABSTRACT

Solute segregation plays a key role in a broad range of phenomena in multiphase materials containing a high density of interfaces, yet the diverse nature of these interfaces makes quantifying and predicting segregation a difficult task. Here we report on the simultaneous segregation of Au atoms to four different interfaces in Fe/Au particles on sapphire – two distinct metal surfaces, a metal-ceramic interface, and a metal-metal grain boundary – resulting in their complete encapsulation. We accessed all of these interfaces *simultaneously* and found substantial differences in their segregation behavior. The metal-ceramic interface exhibited the strongest segregation tendency, followed by the two surfaces, and the grain boundary. The results were analyzed quantitatively by combining experimental, theoretical and *abinitio* computational methods, leading to new synergetic insights into such systems. We then demonstrated how segregation can be directly employed to design the morphology and properties of thermodynamically-stable nanoparticles and thin films.

© 2015 Acta Materialia Inc. Published by Elsevier Ltd. All rights reserved.

1. Introduction

Solute segregation (or Gibbsian adsorption) to surfaces and interfaces is a phenomenon known in materials science for over a century [1]. The thermodynamic driving force for segregation is the reduction of a surface's or interface's energy by its enrichment or depletion with solute atoms, relative to bulk composition. Segregation plays a key role in many phenomena in materials and devices, and can be both beneficial and detrimental. For example, W segregation to the γ/γ' interfaces in Ni-based superalloys used in the aerospace industry improves their mechanical properties [2]; Grain boundary (GB) segregation can result in embrittlement of the material, and a concomitant premature intergranular fracture [3,4]: Electronic and catalytic properties may also be affected by segregation [5,6]. Segregation was also shown to thermodynamicallystabilize nanostructured bulk materials [7,8]. Therefore, the growing interest in multiphase nanostructured materials with their high surface-to-volume ratio, lends increasing importance to studying solute segregation and its effects on interface structure, energy, and properties [9,10]. However, in many cases this proves to be experimentally and computationally difficult, owing to the

* Corresponding author. E-mail address: dor.amram.da@gmail.com (D. Amram).

http://dx.doi.org/10.1016/j.actamat.2015.08.081

1359-6454/© 2015 Acta Materialia Inc. Published by Elsevier Ltd. All rights reserved.

multitude of different types of interfaces in a given material: many surfaces and grain/interphase boundaries of different atomic structures, populating a multi-dimensional space of geometrical degrees of freedom, often co-exist in a single specimen. Although predicting segregation to a certain type of interface (*e.g.* a GB) based on the data for another, more experimentally-accessible interface (*e.g.* a surface) is a tempting concept, such correlations do not always exist [11]. The ability to access several different types of interfaces in the same system simultaneously, and to quantify segregation to them under the same experimental conditions, is therefore necessary. Yet it is considered to be a limiting factor in this field, and previous works in the literature addressed segregation to at most two types of interfaces simultaneously – surfaces and GBs [11,12] or interphase boundaries and GBs [13].

In the case of multi-component thin films segregation also greatly affects both the kinetics of morphology evolution and the equilibrium configuration [14,15]. In a recent work, Au segregation was shown to play a key role in the precipitation of α -Fe from Au solid-solution micro- and nanoparticles obtained by solid-state dewetting of thin films [16]. The strong segregation tendency observed in the Au–Fe system was then employed as a tool for designing core(Fe)-shell(Au) nanoparticles [17]. The Au–Fe alloy presents a convenient model system for segregation studies due to the large difference in surface energies between Fe and Au [18], and the relative ease of detection by electron microscopy methods







owing to the large difference between the atomic numbers of both species.

First-principles computer simulations such as density functional theory (DFT) have also been widely employed for modeling surface and interface segregation [2,19–21]. Au–Fe interfaces have also been studied recently using DFT [22,23]. However, the combined application of experimental, thermodynamic and computational methods for studying segregation to several different, but crystallographically well-defined interfaces in the same material system, is lacking in the literature.

In this work we report on the multilayer segregation of Au to several different types of interfaces in Fe/Au particles on a sapphire substrate: {110} and {100} Fe surfaces, an Fe/Fe GB, and an Fe(110)/ sapphire(0001) interface. Quantitative measurements were performed using transmission electron microscopy (TEM), and were supplemented by thermodynamic modeling and DFT calculations, which supported the experimental findings.

2. Experimental

2.1. Sample preparation

Thin Fe and Au films (5N purity) were deposited by electron beam deposition on *c*-plane sapphire ((0001) single crystal α -Al₂O₃) substrates. Three sample types were prepared by varying the total and relative layer thicknesses (composition): Sample *A* (30 nm; ~74 at.% Fe), sample *B* (30 nm; ~54 at.% Fe) and sample *C* (20 nm; ~54 at.% Fe) (see Table S.1). The complete deposition details are provided in the Supplementary Materials. Annealing was performed in a quartz-tube furnace under forming gas flow (Ar-10%H₂, 5N purity), followed by fast cooling (removal from the hot zone; ~4 °C/s down to 600 °C; ~0.5 °C/s down to 400 °C and a slower cooling rate at lower temperatures). Samples *A*, *B* and *C* were annealed at 900 °C for 24 h. Sample *C* was subsequently annealed at 600 °C for 24 h following cooling from 900 °C at a rate of 5–10 °C/min. A schematic illustration of the experimental procedures is presented in Fig. S.1.

2.2. Characterization methods

The particles were characterized by high-resolution scanning electron microscopy (HRSEM; Zeiss Ultra Plus). Micrographs were taken at an acceleration voltage of 2 kV using an in-lens secondary electron (SE) detector. High-resolution scanning transmission electron microscopy (HRSTEM; FEI Titan 80–300 kV S/TEM) was used to analyze cross-section samples, prepared by the lift-out method [24] in a dual-beam focused ion beam (FIB; FEI Strata 400-S). The FIB lamellae were cut perpendicular to particle facets, and positioned on a Ti grid. Final thinning was performed by Ar⁺ ion milling at an energy of 500 eV (Linda GentleMill3).

2.3. Composition measurement conditions

All composition measurements were performed by energydispersive X-ray spectroscopy (EDXS) in the TEM (STEM mode), at an acceleration voltage of 300 kV. Samples were placed in a low-background specimen holder and were tilted to the [100] zone axis of Fe so that all surfaces/interfaces were edge-on. In the case of grain boundary segregation measurements, it was not possible to bring both Fe precipitates into zone axis simultaneously due the slight misorientation between them which introduces a small, quantifiable error into the calculations. Sample positioning in the holder was such that the tilting angles were identical (within 1°) between samples. The beam parameters (*e.g.* spot size, semi-convergence angle, etc.) were selected to obtain a high count rate of 2000–3000 counts/s whilst maintaining sufficient spatial resolution. Measurement time was 100 s, during which sample drift was at most 1.5 nm, and was corrected throughout.

2.4. Quantification of Au segregation

The analysis is based on an adaptation of the method developed by Walther [25]. For each surface/interface, the (Fe K_{α})/(Au L_{α}) intensity ratio was measured from squares of sizes X_i, varying from 40 nm to 4 nm, centered around each surface/interface (Fig. S.2). The intensity ratio was then plotted as a function of X/2 (Fig. S.3) except for the case of a GB, where it was plotted as a function of X. Linear regression of these plots yielded the effective segregation layer thickness, δ , and the intensity ratio at the segregation layer, *c*, according to:

$$\binom{I_{Fe}^{K_{\alpha}}}{I_{Au}^{L_{\alpha}}} = \frac{X}{\delta} + c$$
 (1)

The effect of beam broadening was also taken into account. Further details regarding Eq. (1) and the broadening are provided in the Supplementary Materials. The measurements were repeated 6–8 times at different positions along each surface/interface. This served to both increase the accuracy and verify the homogeneity of the segregation layer along its length.

The Au coverage, θ , in monolayers was obtained according to:

$$\theta_{Au} = \frac{\delta C_{Au} \rho_{Fe} N_A}{m_{Au} \nu_{Fe}} \tag{2}$$

where *C* is the weight fraction, ρ is the density, *N*_A is Avogadro's constant, *m* is the molecular weight and ν is the planar density. The latter was taken for the pure Fe {110} or {100} planes, depending on the analyzed surface/interface.

The composition was obtained using the Cliff–Lorimer method [26]:

$$\frac{C_{Fe}}{C_{Au}} = k_{Fe-Au} \cdot \frac{I_{Fe}}{I_{Au}} = k_{Fe-Au} \cdot c$$
(3)

where k is a factor which accounts for the difference in atomic numbers, and was determined to be 0.25 \pm 0.04 with the aid of standards (complete details on standard preparation are provided in the Supplementary Materials).

2.5. DFT procedures

We performed spin-polarized total-energy DFT calculations, employing a plane-wave basis set as implemented in the Vienna ab-initio simulation package (VASP) [27], and the MedeA software environment (Materials Design Inc.). We express the exchangecorrelation electronic energy using the PBE energy functional, as implemented in the generalized gradient approximation (GGA) [28], and utilize projector augmented wave (PAW) potentials to represent the core electron density [29]. In our calculations, the plane-waves are spanned with a 450 eV energy cutoff to represent the Kohn-Sham electronic wave functions, and we use a set of uniform Monkhorst-Pack k-point mesh with densities ranging between 0.15 and 0.20 Å⁻¹ to sample the Brillouin zone. Electronic optimization procedures are performed applying energy convergence thresholds ranging between 10^{-6} and 10^{-5} eV. Where relevant, structural relaxation procedures are performed by setting a value of 10^{-6} eV Å⁻¹ for the Hellmann–Feynman force as a Download English Version:

https://daneshyari.com/en/article/1445210

Download Persian Version:

https://daneshyari.com/article/1445210

Daneshyari.com